Advanced Ceramics Progress: Vol. 12, No. 2, (Spring 2026) 11-23

Materials and Energy Research Center
MERC

Contents lists available at ACERP

Advanced Ceramics Progress

Journal Homepage: www.acerp.ir

Original Research Article

Development of a Binder-Free Nanoworm NiOOH/NiO Electrode for Supercapacitors Through Anodic Electrodeposition: The Role of SDS Surfactant

Mahdi Kazazi [a, b, *], Reza Mirzaie [c, d], Akram Ganji Ghelyji [c, d]

[a] *Associate Professor, Department of Materials Engineering, Faculty of Engineering, Malayer University, P.O. Box 65719-95863, Malayer, Iran.*

[b] *Associate Professor, Department of Nanotechnology and Nanomaterials, Faculty of Interdisciplinary Science and Technology, Malayer University, P.O. Box 65719-95863, Malayer, Iran.*

[c] *MSc, Department of Materials Engineering, Faculty of Engineering, Malayer University, P.O. Box 65719-95863, Malayer, Iran.*

[d] *MSc, Department of Nanotechnology and Nanomaterials, Faculty of Interdisciplinary Science and Technology, Malayer University, P.O. Box 65719-95863, Malayer, Iran.*

* Corresponding Author Email: m_kazazi@malayeru.ac.ir (M. Kazazi)

URL: https://www.acerp.ir/article_252665.html

ARTICLE INFO

Article History:

Received 20 August 2026
Revised 29 August 2026
Accepted 08 September 2026

Keywords:

NiOOH,
NiO,
SDS Surfactant,
Electrochemical Deposition,
Supercapacitor

ABSTRACT

The increasing demand for environmentally sustainable energy solutions has driven rapid advances in the development of high-performance supercapacitors. In this study, a nickel oxyhydroxide/nickel oxide (NiOOH/NiO) electrode was fabricated via an electrodeposition method in the presence of SDS surfactant onto a nickel foam substrate, followed by thermal treatment. Structural and morphological characterizations using XRD, FTIR, and FE-SEM confirmed the successful formation of a porous NiOOH structure, with NiO present as a secondary phase. Electrochemical analyses revealed excellent pseudocapacitive behavior, low internal resistance, and a high specific capacitance of 1021 F g^{-1} at 1 A g−1. Moreover, the ion diffusion coefficient, calculated from the Warburg line in EIS measurements, was determined to be 4.51 × 10^{-12} cm^2 s^{-1}, which is significantly higher than that of the electrode fabricated without SDS surfactant (2.24 × 10^{-12} cm^2 s^{-1}), indicating enhanced ion transport facilitated by its porous architecture. The fabricated electrode maintained most of its electrochemical storage capability during prolonged operation, with 91.7% of the initial capacitance remaining following 2,000 consecutive charge–discharge cycles. Such durable cycling performance indicates that the electrode could be a promising option for use in future high-performance supercapacitor devices.

https://doi.org/10.30501/acp.2026.598087.1207

1. INTRODUCTION

The increasing demand for efficient and sustainable energy-storage technologies has stimulated extensive research on supercapacitors. These devices offer high power capability, rapid charge–discharge characteristics, and long cycle life. However, their relatively low energy-storage capability compared with batteries remains a major challenge for applications that require higher energy density. Therefore, considerable attention has been directed toward electrode materials that can provide high charge-storage capability, rapid ion/electron transport, and good structural stability (Abdelaal et al., 2021; Kazazi & Faryabi, 2020; Zhou et al., 2025; Parvizi & Kazazi, 2018).

Please cite this article as: Kazazi, M., Mirzaie, R., & Ganji Ghelyji, A. (2026). Development of a Binder-Free Nanoworm NiOOH/NiO Electrode for Supercapacitors Through Anodic Electrodeposition: The Role of SDS Surfactant. *Advanced Ceramics Progress*, *12*(2), 11-23. https://doi.org/10.30501/acp.2026.598087.1207

Transition-metal oxides and hydroxides are among the most widely studied pseudocapacitive materials. Their reversible redox reactions can provide substantially higher charge-storage capability than conventional electric-double-layer electrodes. Among them, nickel-based compounds, including NiO, Ni(OH)2, and NiOOH, are particularly attractive because of their electrochemical activity, relatively low cost, and favorable theoretical charge-storage characteristics (Hosseinzade et al., 2022; Mazinani et al., 2019; Torknik et al., 2018). However, their practical performance is often limited by low electrical conductivity and incomplete utilization of electrochemically active sites (Budak et al., 2022). Recent studies therefore emphasize conductivity enhancement and morphology engineering. Porous architectures, hierarchical structures, heterostructures, and direct growth on conductive substrates have emerged as effective strategies for improving nickel-based electrodes (Noormohammadi & Naji, 2025; Biswas et al., 2025; Ji et al., 2023; Mohanty et al., 2023; Ojodun et al., 2025).

Recent studies have shown that electrode morphology and architecture strongly influence the charge-storage behavior of nickel-based materials. Hierarchical Ni(OH)2 nanoflake–nanoflower architectures directly grown on three-dimensional nickel foam demonstrated the benefits of an open structure for electrolyte accessibility and redox utilization (Qazi et al., 2025). Similarly, concentration-controlled in-situ growth of NiO on nickel foam produced a morphological evolution from two-dimensional sheets to three-dimensional structures, demonstrating that growth conditions can tailor the architecture and electrochemical behavior of NiO electrodes (Himmah et al., 2024). Other morphology-engineering studies on nickel-based materials have also highlighted the importance of nanoscale structure in controlling electrochemical performance (Noormohammadi & Naji, 2025). These findings reinforce the importance of controlling nanoscale architecture to improve electrolyte accessibility, active-site utilization, and charge-transfer pathways.

Among the available fabrication methods, electrodeposition is particularly attractive for preparing self-supported and binder-free electrodes. The active phase can be directly deposited onto a conductive current collector, providing intimate electrical contact and controllable growth conditions. Anodic electrodeposition has previously been demonstrated as an effective route for producing porous nickel oxide–hydroxide films on nickel foam (Aghazadeh, 2016; Wu et al., 2008). Recent reviews of electrochemical deposition further emphasize its ability to control nucleation, morphology, and the integration of active materials with conductive substrates. Nickel foam also provides a three-dimensional conductive scaffold that supports the active material without polymeric binders and facilitates electron transport throughout the electrode.

In parallel, surfactant-assisted synthesis has emerged as an effective approach for regulating nucleation, particle growth, aggregation, and pore development. Sodium dodecyl sulfate (SDS), an anionic surfactant, is particularly attractive because its amphiphilic nature allows interaction with metal-containing species and can modify the local growth environment. Surfactant effects on electrochemical-induced synthesis of nickel hydroxide have previously been reported (Giarola et al., 2013), while SDS-assisted synthesis of NiO has been shown to produce a distinct porous morphology and improved capacitive behavior (Zhao et al., 2024). More broadly, morphology-controlled NiO studies have demonstrated that surfactant-mediated growth can generate markedly different architectures and electrochemical responses (Maheswari et al., 2021; Murugadoss et al., 2025). Studies using other surfactants have also shown improved performance of nickel-containing electrodes, confirming the importance of surfactant-controlled architecture (Wesley et al., 2024; Ding et al., 2023). These findings indicate that surfactant engineering can be an effective tool for improving the accessibility and utilization of electroactive sites.

Despite substantial progress in morphology engineering, direct-growth strategies, and surfactant-assisted synthesis of nickel-based electrodes, the combined use of SDS-assisted anodic electrodeposition to construct a binder-free, nanoworm-like NiOOH/NiO architecture directly on three-dimensional nickel foam remains insufficiently explored. The present work goes beyond simple morphology modification. It systematically correlates the SDS-induced porous architecture with the charge-storage mechanism, interfacial charge-transfer behavior, and ion-transport characteristics of the electrode. The distinctive aspect of this study is the integration of SDS-mediated morphological control, direct binder-free electrodeposition, and quantitative evaluation of surface-controlled and diffusion-controlled charge storage together with ion-diffusion analysis. This approach provides a clearer structure–electrochemical performance relationship and helps elucidate how surfactant-assisted growth can improve electrolyte accessibility and charge-transport kinetics in NiOOH/NiO-based pseudocapacitive electrodes.

Therefore, the present study focuses on the fabrication of binder-free NiOOH/NiO electrodes directly on three-dimensional nickel foam through anodic electrodeposition in the absence and presence of SDS, followed by mild thermal treatment. The effects of SDS on the structural characteristics, surface morphology, charge-storage behavior, interfacial resistance, and ion-transport properties were systematically investigated using XRD, FTIR, FE-SEM, cyclic voltammetry, galvanostatic charge–discharge, and electrochemical

impedance spectroscopy. Particular emphasis was placed on correlating the SDS-induced nanoworm-like porous architecture with capacitive and diffusion-controlled contributions. The ion-diffusion coefficient was also determined from the Warburg response. This combined analysis was used to clarify the role of SDS in controlling the electrode structure and electrochemical kinetics.

2. MATERIALS AND METHODS

2.1. Chemical Reagents

Sodium acetate, nickel sulfate, and sodium sulfate were purchased from Merck, while sodium dodecyl sulfate (SDS) was obtained from Sigma-Aldrich. All reagents used in the investigation were of analytical-grade purity, and deionized water was consistently used for the preparation and conduct of all experimental procedures.

2.2. Anodic Electrodeposition of NiOOH/NiO

A NiOOH/NiO coating was electrochemically formed on a conductive substrate through an anodic deposition process, with sodium dodecyl sulfate (SDS) incorporated into the deposition medium as a surfactant. Since impurities on the conductive substrate can introduce significant experimental errors, a pretreatment step was implemented. Prior to deposition, a nickel foam substrate (1 × 1 cm^2) was immersed and continuously stirred in 6 M HCl for 4 h to eliminate impurities and contaminants from its surface. Following acid treatment, the foam was thoroughly rinsed with deionized water in several stages and subsequently dried at 80 °C overnight. Then, the composite electrode was synthesized via an anodic electrochemical deposition process using a two-electrode configuration. The electrochemical cell was configured with nickel foam as the working electrode, while a stainless-steel electrode functioned as the counter electrode. The electrodes were aligned in a parallel orientation with a fixed interelectrode distance of 1 cm. Electrodeposition was performed at ambient temperature using a fixed current density of 20 mA cm^{-2} for 10 min. During the process, the electrolyte was allowed to contact both faces of the nickel foam substrate, enabling deposition across the exposed surfaces. The electrodeposition process was performed without deaeration and under magnetic stirring to reduce concentration polarization. The electrolyte solution used for the deposition consisted of 0.13 M nickel sulfate, 0.13 M sodium acetate, 0.26 M SDS, and 0.1 M sodium sulfate. The initial pH of the electrolyte was measured to be about 6. Subsequently, the as-prepared films were subjected to annealing at 200 °C for 90 min. The mass loading of the active material was measured to be about 5 mg for each electrode after the calcination treatment.

2.3. Structural and Electrochemical Properties of the Electrodes

X-ray diffraction (XRD, Unisantis XMD-300, Georgsmarienhütte, Germany) analysis was employed to determine the crystalline phases of the synthesized electrodes prepared in the absence and presence of SDS surfactant. The surface architecture of the synthesized NiOOH/NiO electrodes was investigated using field-emission scanning electron microscopy (FESEM; Mira 3-XMU, Tescan, Brno, Czech Republic). FTIR analysis was also performed using a Bruker Alpha 2 spectrometer (Bruker Optics, Ettlingen, Germany) to determine the characteristic functional groups and chemical species associated with the prepared electrode. The capacitive performance of the fabricated electrodes was evaluated using an Autolab workstation (GSTAT 302N, Metrohm, Barendrecht, Netherlands) in a 2 M KOH aqueous electrolyte. Electrochemical characterization was conducted using a standard three-electrode cell, with the prepared electrode serving as the working electrode, a platinum plate functioning as the auxiliary electrode, and Ag/AgCl used as the reference electrode. The electrochemical performance of the fabricated electrodes was evaluated through cyclic voltammetry (CV), galvanostatic charge–discharge (GCD), durability cycling tests, and electrochemical impedance spectroscopy (EIS) to determine their potential for supercapacitor applications.

3. RESULTS AND DISCUSSION

3.1. Electrode Fabrication and Characterization

Figure 1. Graphical depiction of the sequential steps involved in producing the binder-free NiOOH/NiO/SDS electrode.

Figure 1 schematically depicts the fabrication procedure for NiOOH/NiO/SDS thin films deposited on nickel foam. As shown, the synthesis of the binder-free NiOOH/NiO/SDS electrode consists of three sequential stages: substrate pretreatment, anodic electrodeposition of active material nanoworms, and subsequent calcination. Substrate pretreatment was performed to remove oxide layers from the surface of the nickel foam. SDS surfactant was added to the plating solution to improve the morphological characteristics of the active material by producing a more porous structure, thereby enhancing its electrochemical activity.

X-ray diffraction (XRD) stands as a highly effective analytical technique for elucidating the crystalline structure and phase composition of materials. Figure 2 presents the XRD patterns corresponding to the bare nickel foam, NiOOH/NiO, and NiOOH/NiO/SDS electrodes, electrochemically deposited onto nickel foam in the absence and presence of SDS surfactant, respectively. The intense diffraction peaks observed at approximately 44.5° and 51.8° are attributed to the (111) and (200) planes of the face-centered cubic (fcc) Ni substrate, respectively, in accordance with JCPDS Card No. 04-0850. These strong reflections originate from the nickel foam current collector and are observed in both deposited electrodes. It can be seen that both XRD patterns related to the NiOOH/NiO and NiOOH/NiO/SDS electrodes are similar, indicating that the crystal structure of the NiOOH/NiO active material remains unchanged during the electrodeposition process with SDS serving as the surfactant. The peaks observed at 20.8°, 35.0°, 39.9°, 61.3°, and 64.7° are indexed to the (120), (101), (230), (301), and (181) crystal planes of NiOOH (Wu et al., 2008). These diffraction features provide clear evidence for the development of a crystalline NiOOH phase after annealing the material at 200 °C. Furthermore, the peaks observed at 2θ = 37.7°, 43.3°, and 63.5° can be indexed to the (111), (200), and (220) crystallographic planes of NiO, respectively, in accordance with the standard JCPDS reference pattern No. 47-1049 (Aghazadeh, 2016; Mallick et al., 2009; Noukelag et al., 2021). The presence of these characteristic reflections indicates that NiO is formed as a secondary phase in the electrode, coexisting with the dominant NiOOH phase.

FTIR analysis was carried out to identify the characteristic chemical bonds and functional groups associated with the synthesized electrode materials. The spectra presented in Figure 3 compare the responses of pristine SDS with those of the NiOOH/NiO and SDS-modified NiOOH/NiO electrodes. The active materials were mechanically removed from the corresponding electrode surfaces prior to analysis.

For the sample prepared without SDS, several characteristic absorption features were detected. The broad absorption centered near 3400 cm^{-1} is related to O–H stretching and is mainly associated with adsorbed moisture. The feature at 1638 cm^{-1} can be assigned to the bending vibration of H_2O molecules. Another band, located at approximately 1422 cm^{-1}, is associated with the rotational motion of water species present within the material. The absorption observed around 1140 cm^{-1} is related to sulfate ion vibrations, indicating that a small amount of sulfate species remains in the electrode.

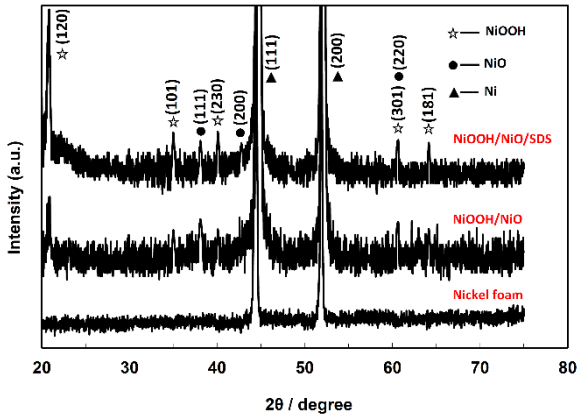

Figure 2. X-ray diffraction patterns obtained for the nickel foam substrate, NiOOH/NiO electrode, and SDS-modified NiOOH/NiO electrode.

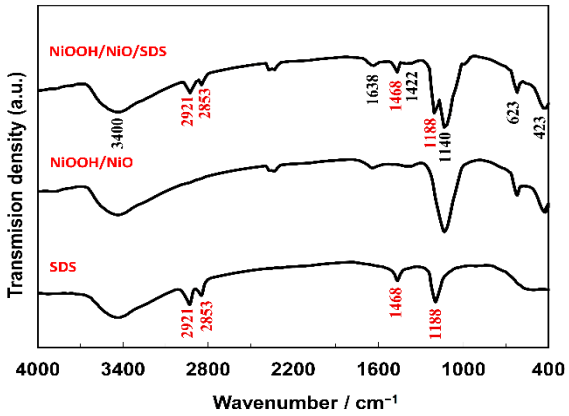

Figure 3. FTIR spectra recorded for SDS, NiOOH/NiO, and NiOOH/NiO/SDS electrode materials collected from the respective electrode surfaces.

The lower-wavenumber region provides further information regarding the nickel-containing phases. The absorption band near 623 cm^{-1} can be attributed to Ni–O-related vibrations associated with the NiOOH phase, consistent with previously reported FTIR characteristics of NiOOH (Kim et al., 2025). In contrast, the band at approximately 423 cm^{-1} is assigned to the Ni–O stretching vibration of NiO, in agreement with previously reported FTIR results for NiO materials (Mahaleh et al., 2008). Thus, the FTIR results are consistent with the coexistence of NiOOH and NiO in the electrode.

A different spectral response was observed after introducing SDS during electrode preparation. The NiOOH/NiO/SDS sample exhibits an additional absorption near 1188 cm^{-1}, which is attributed to S=O stretching vibration. Furthermore, the bands appearing at 1468 and 2921 cm^{-1} are assigned to symmetric and asymmetric C–H stretching vibrations, respectively. These characteristic features correspond well with those observed for the pristine SDS spectrum in Figure 3 (Lun et al., 2013; Zhang, 2015; Al-Gaashani et al., 2019; Giarola et al., 2013).

Taken together, the FTIR findings confirm the characteristic bonding environments of the NiOOH/NiO system and provide additional spectral evidence for the successful incorporation of SDS into the electrode material. The appearance of the characteristic SDS-related vibrations in the modified sample confirms the influence of the surfactant during electrode fabrication.

FE-SEM serves as a complementary and indispensable technique for elucidating the surface morphology of the synthesized NiOOH/NiO electrodes. Figure 4 presents FE-SEM micrographs of bare nickel foam, NiOOH/NiO, and NiOOH/NiO/SDS electrodes at various magnifications, highlighting their morphological features. As seen in Figure 4a, nickel foam has a three-dimensional porous structure, which makes it a suitable substrate for active material deposition. As depicted in Figure 4b,c, a uniform and relatively dense coating of active material nanoparticles is deposited on the surface of the substrate, forming the NiOOH/NiO electrode. In contrast, FE-SEM images of the NiOOH/NiO/SDS electrode (Figure 4d–f) indicate that the active material nanoworms synthesized in the presence of SDS are homogeneously dispersed over the full exposed area of the substrate, forming a porous and conductive network through the electrochemical deposition process. Based on the SEM images, the electrode structure became more porous in the presence of SDS surfactant. This well-organized porous structure not only facilitates efficient electron transport but also provides a multitude of intercalation sites and a favorable microstructural architecture, thus contributing to a substantial improvement in the electrochemical characteristics of the resulting supercapacitor. This unique morphology of the NiOOH/NiO/SDS layer exhibits a synergistic effect, contributing to superior electrochemical activity within aqueous electrolytes for energy storage applications.

Such morphological characteristics result in an enlarged electrode–electrolyte interfacial area, increased active material volume, and reduced diffusion pathways for ion transport. These features collectively promote improved electrolyte diffusion kinetics and enhanced wettability of the active electrode surface, thus playing a pivotal role in faradaic charge storage mechanisms. Consequently, the electrochemically active NiOOH/NiO material demonstrates superior capacitive behavior, with

substantial improvements in charge/discharge efficiency and overall supercapacitor performance.

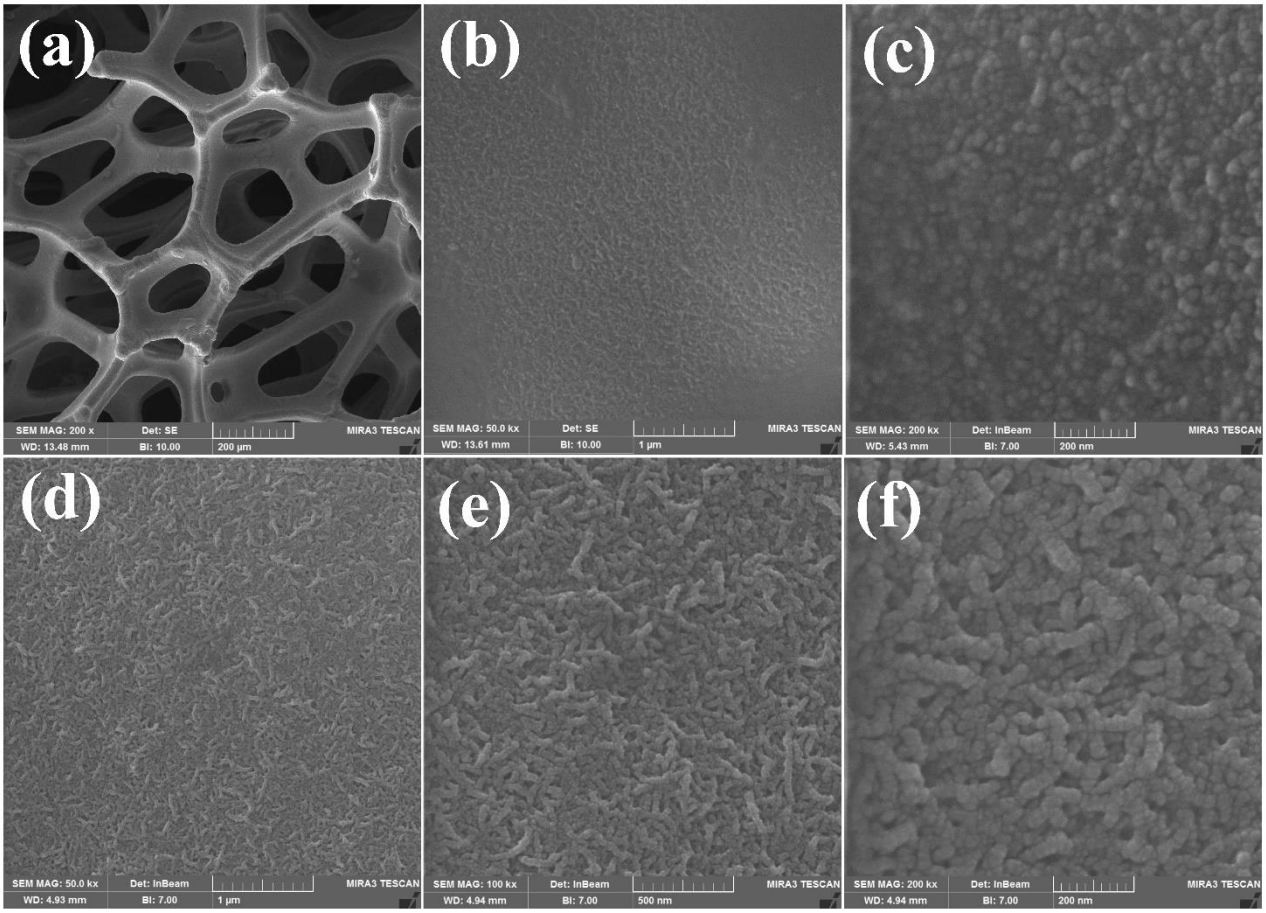

Figure 4. FESEM images of the (a) NF, (b, c) NiOOH/NiO, and (d–f) NiOOH/NiO/SDS electrodes at various magnifications.

3.2. Electrochemical Measurements

The role of SDS in modifying the charge-storage characteristics of the NiOOH/NiO electrode was examined through CV and GCD measurements. Particular attention was given to the changes in electrochemical response associated with the structural and morphological effects of the surfactant. The CV measurements were performed in 2 M aqueous KOH using Ag/AgCl as the reference electrode.

The electrochemical responses obtained at 20 mV s^{-1} over the 0–0.7 V potential range are compared in Figure 5a. The profiles of both electrodes exhibit pronounced oxidation and reduction features rather than the rectangular shape normally associated with purely electric double-layer capacitance. The presence of these faradaic peaks confirms that reversible redox reactions contribute substantially to the charge-storage process, which is characteristic of pseudocapacitive behavior.

A comparison of the enclosed CV areas reveals a clear difference between the two electrodes. The NiOOH/NiO/SDS sample exhibits a considerably greater integrated area than the unmodified NiOOH/NiO electrode, indicating a larger charge-storage capacity and, consequently, higher specific capacitance. The SDS-containing electrode also shows a reduced separation between its oxidation and reduction potentials. This smaller peak-to-peak difference is indicative of improved reversibility and more favorable electrochemical reaction kinetics.

The effect of scan rate on the modified electrode was subsequently investigated, with the corresponding CV profiles presented in Figure 5b. Increasing the scan rate from 10 to 50 mV s^{-1} causes the oxidation peak to move toward higher potentials, while the reduction peak shifts toward lower potentials. The observed polarization at elevated scan rates can be associated with the limited time available for electrolyte ions to migrate and access the electrochemically active regions of the electrode.

Nevertheless, the overall shape of the CV profiles is largely preserved as the scan rate increases, and the oxidation–reduction features remain well defined. The retention of this characteristic response suggests that the NiOOH/NiO/SDS electrode possesses good rate

capability and reversible redox activity. Its favorable high-rate behavior can be linked to effective electrolyte-ion movement within the electrode structure and relatively low resistance to charge transport, allowing the material to undergo rapid charging and discharging.

The electrochemical response of a pseudocapacitive material can be separated into surface-controlled and diffusion-controlled contributions. The former is associated primarily with rapid charge accumulation at accessible electrode surfaces, whereas the latter involves the transport of electrolyte ions into the electrode and their participation in reversible faradaic processes. Within the Trasatti framework (Bhojane, 2022), the measured charge (q) is consequently represented as the combined contribution of (q_c), corresponding to the capacitive process, and (q_d), associated with diffusion-controlled storage:

$$q = q_d + q_c \quad (1)$$

For pseudocapacitive systems, the diffusion-related contribution depends on the inverse square root of the scan rate (Kazazi & Ghelyji, 2024). On this basis, Eq. (1) can be rearranged into the following linear form:

$$q = A\left(v^{-1/2}\right) + q_c \quad (2)$$

where (A) represents a constant related to the diffusion-controlled contribution. Based on the Trasatti method, the measured capacitance was plotted as a function of the inverse square root of the scan rate to distinguish the surface-controlled and diffusion-controlled contributions (Figure 5c). A highly linear relationship was obtained for the NiOOH/NiO/SDS electrode, with a coefficient of determination of (R2 = 0.9895), demonstrating a strong correlation and good fitting quality. The high (R2) value confirms the validity of the linear fitting and supports the reliability of the extrapolation used to estimate the theoretical surface-controlled capacitive contribution. The extrapolated intercept corresponds to a theoretical surface-controlled capacitive contribution of 432 F g^{-1}. The contribution arising from ion diffusion was then determined at each scan rate by taking the difference between the measured total capacitance and the calculated surface-controlled capacitive contribution. The resulting variation in the diffusion-controlled capacitance is presented in Figure 5d.

A progressive reduction in the diffusion contribution is evident as the scan rate is increased. This behavior can be explained by the restricted time available for KOH electrolyte ions to penetrate the electrode and reach electrochemically active sites during rapid potential sweeping. Consequently, at elevated scan rates, the charge-storage process increasingly relies on the faster surface-controlled contribution rather than ion diffusion into the bulk of the NiOOH/NiO/SDS structure.

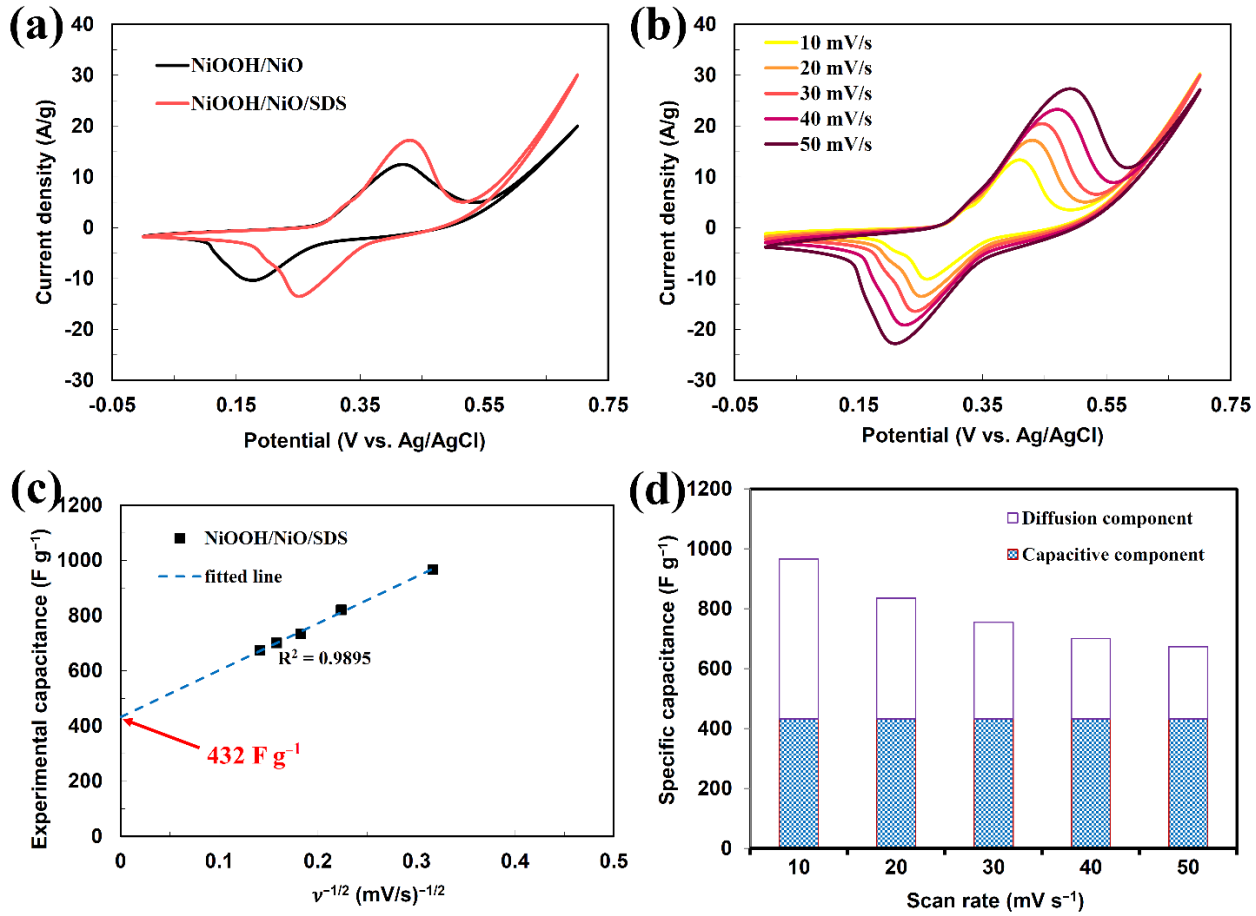

Figure 5. (a) Comparative cyclic voltammograms obtained for the NiOOH/NiO and SDS-modified NiOOH/NiO electrodes at 20 mV s^{-1}; (b) scan-rate-dependent CV responses of the NiOOH/NiO/SDS electrode; (c) plot of the measured capacitance versus $v^{-1/2}$ for evaluating the theoretical surface-controlled capacitance; and (d) variation of the surface-capacitive and diffusion-controlled contributions with increasing scan rate for the NiOOH/NiO/SDS electrode.

The charge-storage capability of the deposited materials was further examined by galvanostatic charge–discharge measurements. Unlike CV, GCD testing allows the specific capacitance of an electrode to be quantitatively determined under a fixed applied current. The resulting potential–time responses for NiOOH/NiO and NiOOH/NiO/SDS are presented in Figures 6a and 6b, respectively, for current densities between 1 and 10 A g^{-1}. Both electrodes exhibit distinct discharge characteristics. In particular, the voltage loss observed at the onset of discharge is smaller for the SDS-containing electrode. This reduced IR drop is indicative of lower ohmic resistance and more effective electronic conduction within the modified electrode. The charge and discharge curves also contain discernible plateaus, reflecting the involvement of reversible faradaic reactions rather than solely electrostatic charge accumulation. Such behavior is consistent with the pseudocapacitive response expected from nickel oxide/hydroxide-based materials.

Another notable difference is the substantially longer discharge period observed for NiOOH/NiO/SDS. Under identical current conditions, a longer discharge duration corresponds to a greater quantity of stored charge and therefore a higher specific capacitance. The improvement achieved after SDS incorporation is likely related to changes in the growth mechanism and surface architecture during electrodeposition. The surfactant can modify the nucleation and development of the deposited phase, producing a structure with enhanced porosity. Increased pore accessibility can facilitate the movement of electrolyte ions and improve contact between the electrolyte and electrochemically active regions.

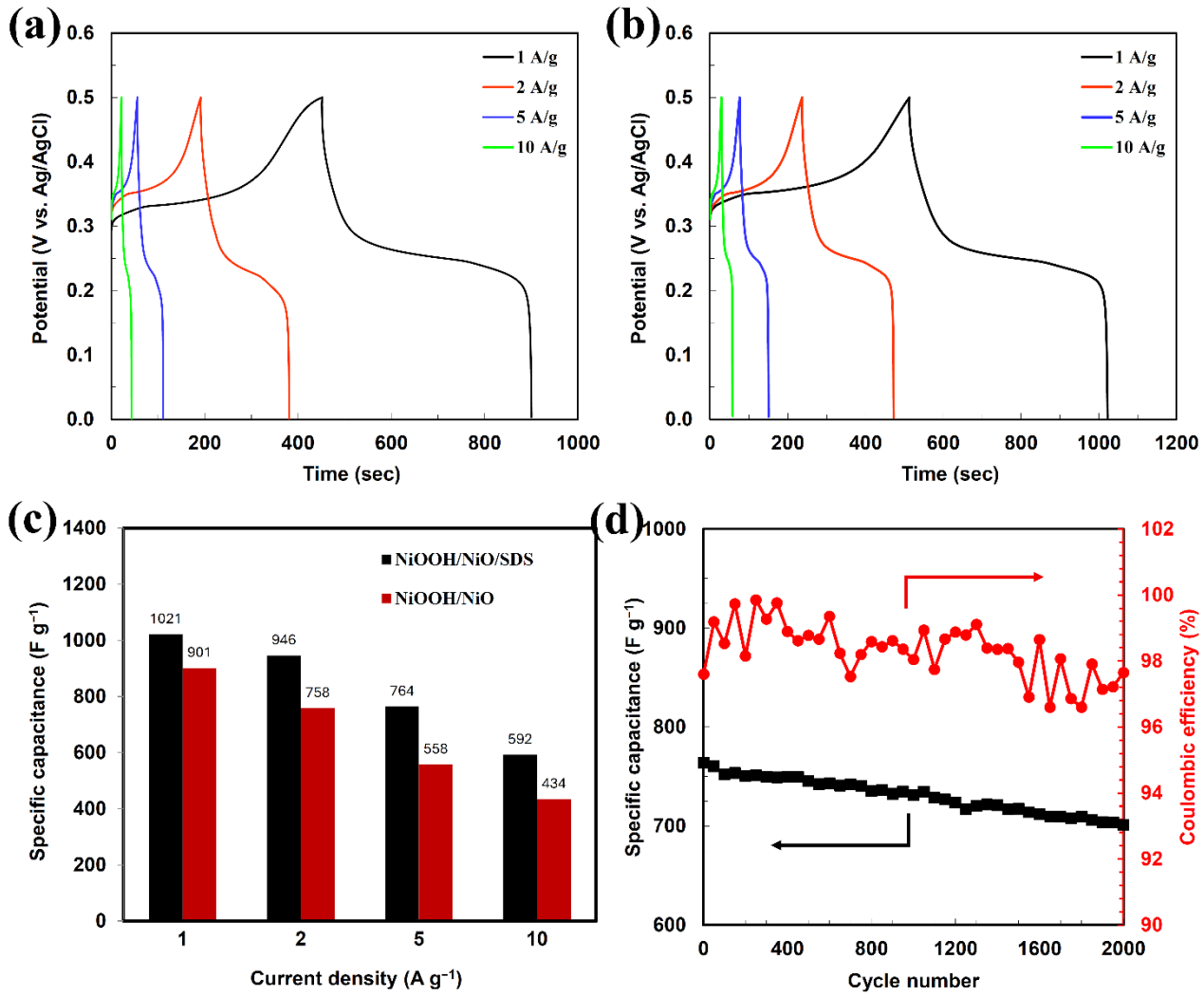

Figure 6. (a, b) Galvanostatic charge–discharge profiles of the NiOOH/NiO and NiOOH/NiO/SDS electrodes, respectively, recorded at different current densities; (c) variation of the specific capacitance as a function of applied current density for both electrodes; and (d) capacitance retention and Coulombic efficiency of the NiOOH/NiO/SDS electrode during 2000 consecutive cycles at 5.0 A g^{-1}.

The specific capacitance was obtained from the discharge branches using Eq. (3), following the methodology reported by (Wang & Zheng, 2024):

$$C_s = \frac{i \times \Delta t}{m \times \Delta V} \quad (3)$$

Here, (i) denotes the applied discharge current, (Δt) is the corresponding discharge duration, (m) represents the mass of active material deposited on the nickel foam, and (ΔV) is the potential range used during the measurement.

According to Figure 6c, the NiOOH/NiO/SDS electrode reaches 1021 F g^{-1} at 1 A g^{-1}. When the current density is increased to 2, 5, and 10 A g^{-1}, the calculated capacitance decreases to 946, 764, and 592 F g^{-1}, respectively. At every investigated current density, the SDS-modified electrode exhibits greater capacitance than the corresponding NiOOH/NiO electrode.

The decline in capacitance at increasing current density is characteristic of porous faradaic electrodes. Rapid current application limits the time available for electrolyte ions to migrate through the electrode and reach less accessible active regions. Therefore, under high-current operation, the redox processes are concentrated mainly at the outer surface and easily accessible pores. Conversely, slower discharge conditions provide sufficient time for ions to penetrate deeper into the electrode, allowing a greater proportion of the active material to contribute to charge storage.

The performance of the present NiOOH/NiO/SDS electrode was compared with previously reported nickel-based oxide and hydroxide electrodes, as summarized in Table 1. The material produced in this work achieves a specific capacitance of 1021 F g^{-1} at 1 A g^{-1} and retains 91.7% of its initial capacitance following 2000 cycles. These characteristics compare favorably with many of the previously reported systems, demonstrating the

potential advantage of combining NiOOH/NiO with SDS-assisted electrochemical deposition.

Table 1. Comparative overview of the electrochemical characteristics of the NiOOH/NiO/SDS electrode developed in this study and previously reported nickel-based oxide/hydroxide electrodes.

Electrode Material	Substrate	Specific Capacitance	Cycling Stability	Methods	Ref.
Ni-Co$(OH)_2$	Nickel foam	584 F g^{-1} at 1 mA cm^{-2}	87.8% (2000 cycles)	Hydrothermal	(Pawar et al., 2025)
$CoNi_{(1-x)}Mo_xOH$	carbon cloth	293 F g^{-1} at 1 A g^{-1}	80% (1200 cycles)	Hydrothermal	(Mishra et al., 2025)
$Ni(OH)_2$-activated carbon	Nickel foam	391 F g^{-1} at 1 A g^{-1}	96.6% (5000 cycles)	Hydrothermal	(Wongsaprom et al., 2025)
NiO	Nickel foam	855 F g^{-1} at 0.5 A g^{-1}	75% (5000 cycles)	solvothermal	(Shaikh et al., 2026)
PANI-NiO	stainless steel	522 F g^{-1} at 1 A g^{-1}	79.5% (3000 cycles)	chemical oxidation technique	(Patil et al., 2024)
Ni_3Si_2/NiOOH/Graphene	Nickel	1193 F g^{-1} at 1 A g^{-1}	90.7% (6000 cycles)	Chemical vapor deposition	(Ning et al., 2020)
NiOOH/NiO/SDS	Nickel foam	1021 F g^{-1} at 1 A g^{-1}	91.7% (2000 cycles)	Electrochemical deposition	This work

Long-term stability is particularly important when electrode materials are considered for repeated energy-storage operation. The durability of the NiOOH/NiO/SDS electrode was therefore tested by performing 2000 consecutive GCD cycles at 5 A g^{-1} in 2 M KOH. The resulting capacitance-retention profile is shown in Figure 6d. Only a limited decrease in capacitance occurs during the cycling experiment, with 91.7% of the initial value preserved after 2000 cycles. The high retention indicates that the electrode maintains its electrochemical functionality despite repeated charging and discharging. The stability can be related, at least in part, to the morphology generated in the presence of SDS, which promotes accessible pathways for electrolyte ions and facilitates charge transport throughout the electrode.

Coulombic efficiency was evaluated simultaneously with capacitance retention. Throughout the 2000-cycle experiment, the Coulombic efficiency remained higher than 96%, demonstrating that the charge-storage reactions are highly reversible. The combination of high capacitance retention and favorable Coulombic efficiency confirms the suitability of the binder-free NiOOH/NiO/SDS architecture for repeated electrochemical operation.

The interfacial resistance and ion-transport characteristics of the electrodes were examined by electrochemical impedance spectroscopy. Figure 7a presents the Nyquist responses recorded for NiOOH/NiO and NiOOH/NiO/SDS between 100 kHz and 100 mHz at open-circuit potential. Two characteristic portions can be distinguished in both spectra. The feature appearing at high frequency is represented by a semicircle and is associated with charge-transfer resistance at the electrode/electrolyte interface. At lower frequencies, the impedance curves develop into inclined linear regions, commonly attributed to the Warburg response arising from ion diffusion.

The SDS-modified electrode exhibits a noticeably smaller high-frequency semicircle than the unmodified material. This behavior indicates a reduction in charge-transfer resistance and suggests that electron transfer across the electrode/electrolyte interface is facilitated by the structural modification induced by SDS. The low-frequency region also shows a steeper slope for NiOOH/NiO/SDS, which is consistent with improved electrolyte-ion diffusion (Yang et al., 2025).

To quantify the ion-transport behavior, the diffusion coefficient was calculated from the Warburg response using Eq. (4), according to the approach reported by (Panigrahi et al., 2020; Shahzad et al., 2025):

$$D = 0.5\left(\frac{RT}{An^2F^2\sigma_w C}\right)^2 \quad (4)$$

The Warburg coefficient, (σ_w), used in this calculation was obtained from the linear dependence of (Z_{re}) on the reciprocal square root of angular frequency, as expressed by Eq. (5):

$$Z_{re} = R_D + R_L + \sigma_w \omega^{-1/2} \quad (5)$$

Figure 7b presents the corresponding low-frequency plots used to determine the Warburg slopes. The calculated diffusion coefficients are 2.24 × 10^{-12} cm^2 s^{-1} for NiOOH/NiO and 4.51 × 10^{-12} cm^2 s^{-1} for NiOOH/NiO/SDS. The substantially larger diffusion coefficient obtained for the SDS-containing electrode suggests that electrolyte ions can migrate more readily through its structure. This behavior is plausibly associated with the porous morphology promoted by SDS during deposition. Greater pore accessibility provides additional channels for electrolyte penetration and facilitates contact between ions and active redox sites. Consequently, the improved ion-transport characteristics help explain the enhanced capacitance and electrochemical response observed for the NiOOH/NiO/SDS electrode.

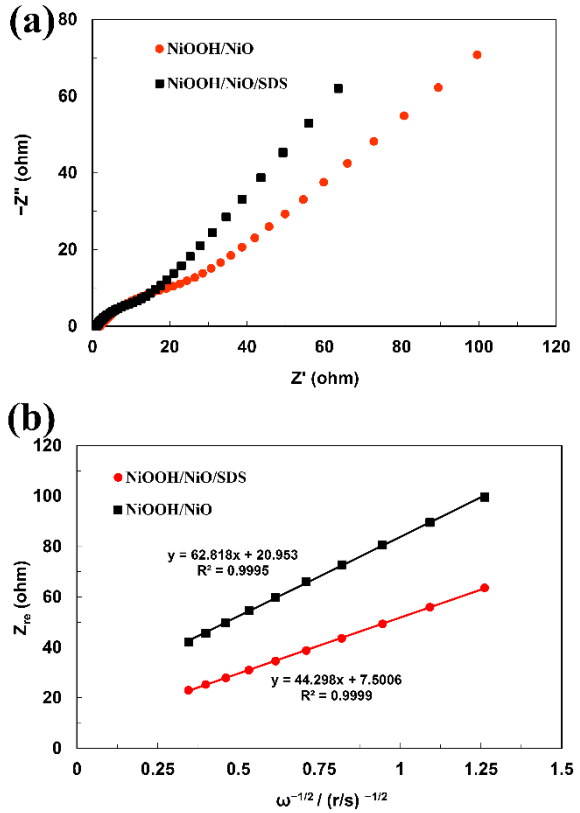

Figure 7. (a) Nyquist impedance spectra recorded for the NiOOH/NiO and NiOOH/NiO/SDS electrodes; (b) linear dependence of the real impedance component (Z_{re}) on ($\omega^{-1/2}$) in the low-frequency region.

4. CONCLUSION(S)

The results of this study demonstrate the successful preparation of binder-free NiOOH/NiO electrodes directly on nickel foam using electrochemical deposition, with SDS employed to modify the deposition process. Subsequent thermal treatment produced the desired electrode structure. The introduction of SDS had a pronounced effect on the resulting morphology, favoring the development of a porous and more uniformly distributed active layer. This structural modification improved the accessibility of the electrolyte and facilitated both ionic and electronic transport. The enhanced architecture was reflected in the electrochemical measurements. The NiOOH/NiO/SDS electrode delivered a maximum specific capacitance of 1021 F g^{-1} at 1 A g^{-1}. In addition, an ion-diffusion coefficient of 4.51 × 10^{-12} cm^2 s^{-1} was obtained, suggesting efficient electrolyte-ion movement through the electrode. The modified electrode also exhibited excellent durability during repeated operation, preserving 91.7% of its initial capacitance after 2000 continuous charge–discharge cycles. These findings confirm the effectiveness of SDS-assisted synthesis in improving the electrochemical properties of NiOOH/NiO electrodes, positioning them as viable materials for high-performance supercapacitor systems.

ACKNOWLEDGEMENTS

The authors sincerely appreciate the technical support and assistance provided by Mostafa Mirshahvalad at the Central Laboratory of Malayer University during this research.

REFERENCES

1. Abdelaal, M.M.; Hung, T.-C.; Mohamed, S.G.; Yang, C.-C.; Huang, H.-P.; Hung, T.-F. A (2021). Comparative Study of the Influence of Nitrogen Content and Structural Characteristics of NiS/Nitrogen-Doped Carbon Nanocomposites on Capacitive Performances in Alkaline Medium. *Nanomaterials* 11, 1867. https://doi.org/10.3390/nano11071867.

2. Aghazadeh, M. (2016). Synthesis, characterization, and study of the supercapacitive performance of NiO nanoplates prepared by the cathodic electrochemical deposition-heat treatment (CED-HT) method. *J. Mater. Sci. Mater. Electron.* 28, 3108–3117. https://doi.org/10.1007/s10854-016-5899-x.

3. Al-Gaashani, R.; Najjar, A.; Zakaria, Y.; Mansour, S.; Atieh, M.A. (2019). XPS and structural studies of high-quality graphene oxide and reduced graphene oxide prepared by different chemical oxidation methods. *Ceram. Int.* 45, 14439–14448. https://doi.org/10.1016/j.ceramint.2019.04.165.

4. Bhojane, P. (2022). Recent advances and fundamentals of Pseudocapacitors: Materials, mechanism, and its understanding. *J. Energy Storage* 45, 103654. https://doi.org/10.1016/j.est.2021.103654.

5. Biswas, P.; Dev, A.; Kumar, P.; Kour, P.; Kashyap, Y.; Pandey, R.K.; Kar, M. (2025). Morphology-controlled Ag modified mixed valent manganites as a supercapacitor electrode material with adequate energy, power density, and large capacity retention. *J. Alloys Compd.* 1037, 182323. https://doi.org/10.1016/j.jallcom.2025.182323.

6. Budak, Ö.; Uğuz, Ö.; Koca, A. (2022). Simultaneous electrochemical deposition of nickel cobalt oxide-reduced graphene oxide composites for high performance asymmetric supercapacitors. *J. Energy Storage* 47, 103538. https://doi.org/10.1016/j.est.2021.103538.

7. Ding, Q.; Li, J.; Li, S.; Wang, J.; Huang, W.; Sun, S.; Xu, Y.; Li, H. (2023). Preparation of novel composites based on SDS intercalated CoNiFe–LDH and carbon materials for advanced asymmetric supercapacitors. *J. Energy Storage* 67, 107556. https://doi.org/10.1016/j.est.2023.107556.

8. Giarola, D.A.; da Silva, P.R.C.; Urbano, A.; de Oliveira, F.M.; Tarley, C.R.T.; Dall'aNtonia, L.H. (2013). Surfactant effect on electrochemical-induced synthesis of α-Ni(OH)2. *J. Solid State Electrochem.* 18, 497–504. https://doi.org/10.1007/s10008-013-2280-3.

9. Himmah, S.W.; Septiani, N.L.W.; Wustoni, S.; Raissa; Hardianto, Y.P.; Kim, H.; Rinawati, M.; Yeh, M.-H.; Yuliarto, B.; Nuruddin, A. (2024). In-Situ Growth of 2D to 3D NiO on Nickel Foam with Enhanced Capacity Retention as Battery-Type Electrode for Asymmetric Supercapacitor. *Chem. Nano. Mat.* 10, e202400210. https://doi.org/10.1002/cnma.202400210.

10. Hosseinzade, M.R.; Naji, L.; Hasannezhad, F. (2022). Electrochemical deposition of NiO bunsenite nanostructures with different morphologies as the hole transport layer in polymer solar cells. *J. Electroanal. Chem.* 926, 116955. https://doi.org/10.1016/j.jelechem.2022.116955.

11. Ji, J.; Park, S.; Choi, J.H. (2023). Morphology Engineering of Hybrid Supercapacitor Electrodes from Hierarchical Stem-like Carbon Networks with Flower-like MoS2 Structures. *ACS Omega* 8, 16833–16841. https://doi.org/10.1021/acsomega.3c00445.

12. Kazazi, M.; Faryabi, M. (2020). Electrochemically anchored manganese hexacyanoferrate nanocubes on three-dimensional porous graphene scaffold: Towards a potential application in high-performance asymmetric supercapacitors. *J. Power Sources* 449, 227510. https://doi.org/10.1016/j.jpowsour.2019.227510.

13. Kazazi, M.; Ghelyji, A.G. (2024). Enhanced Pseudocapacitive Performance of Electrochemically Deposited α-NiMoO4 Nanoworms on 3D Reduced Graphene Oxide Scaffold. *JOM* 77, 529–538. https://doi.org/10.1007/s11837-024-06969-6.

14. Kim, J.; Yoo, J.; Lee, K. (2025). Unveiling the Role of Electrocatalysts Activation for Iron-Doped Ni Oxyhydroxide in Enhancing the Catalytic Performance of Oxygen Evolution Reaction. *Energy Environ. Mater.* 8(2), e12827. https://doi.org/10.1002/eem2.12827.

15. Lun, H.; Ouyang, J.; Yang, H. (2013). Enhancing dispersion of halloysite nanotubes via chemical modification. *Phys. Chem. Miner.* 41, 281–288. https://doi.org/10.1007/s00269-013-0646-9.

16. Mahaleh, B.M.M.; Sadrnezhaad, S.K.; Hosseini, D. (2008). NiO Nanoparticles Synthesis by Chemical Precipitation and Effect of Applied Surfactant on Distribution of Particle Size. *J. Nanomater.* 470595. https://doi.org/10.1155/2008/470595.

17. Maheswari, N.; Nithya, R.; Ahamed, S.R.; Kalpana, S. (2021). Surfactant concentration influences the morphology and electrochemical properties of CuO Nanoparticles synthesized via microwave method. *Mater. Today Proc.* 45, 4020–4025. https://doi.org/10.1016/j.matpr.2020.10.751.

18. Mallick, P.; Rath, C.; Biswal, R.; Mishra, N.C. (2009). Structural and magnetic properties of Fe doped NiO. *Indian J. Phys.* 83, 517–523. https://doi.org/10.1007/s12648-009-0012-4.

19. Mazinani, B.; Kazazi, M.; Mobarhan, G.; Shokouhimehr, M. (2019). The Combustion Synthesis of Ag-Doped MnCo2O4 Nanoparticles for Supercapacitor Applications. *JOM* 71, 1499–1506. https://doi.org/10.1007/s11837-019-03387-x.

20. Mishra, T.T.; Chakraborty, M.; Parashar, C.K.; Mahanta, J.; Pattader, P.S.G.; Roy, D. (2025). Rational design of CoNiMo trimetallic hydroxide nanostructured flexible electrode for supercapacitor application. *J. Mater. Sci. Mater. Electron.* 36, 180. https://doi.org/10.1007/s10854-025-14234-y.

21. Mohanty, A.; Kang, K.; Saravanakumar, B.; Ramadoss, A.; Jang, J. (2023). Morphology Control of Mixed Metallic Organic Framework for High-Performance Hybrid Supercapacitors. *Small* 20, e2308771. https://doi.org/10.1002/smll.202308771.

22. Murugadoss, G.; Kandhasamy, N.; Zaporotskova, I.V.; Venkatesh, N.; Salla, S.; Pandurengan, S. (2025). Morphology-Controlled Nickel Oxide Nanostructures: Unlocking High-Performance Supercapacitor Applications. *Chem. Phys. Impact* 10, 100888. https://doi.org/10.1016/j.chphi.2025.100888.

23. Ning, J.; Xia, M.; Wang, D.; Feng, X.; Zhou, H.; Zhang, J.; Hao, Y. (2020). Superior Pseudocapacitive Storage of a Novel Ni3Si2/NiOOH/Graphene Nanostructure for an All-Solid-State Supercapacitor. *Nano-Micro Lett.* 13, 2. https://doi.org/10.1007/s40820-020-00527-w.

24. Noormohammadi, E.; Naji, L. (2025). Morphology engineering of NiCo2S4 for supercapacitor applications: A study on spherical and cubic structures. *J. Energy Storage* 131, 117580. https://doi.org/10.1016/j.est.2025.117580.

25. Noukelag, S.; Mohamed, H.; Moussa, B.; Razanamahandry, L.; Ntwampe, S.; Arendse, C. (2021). Structural and optical investigations of biosynthesized bunsenite NiO nanoparticles (NPs) via an aqueous extract of Rosmarinus officinalis (rosemary) leaves. *Mater. Today Proc.* 36, 245–250. https://doi.org/10.1016/j.matpr.2020.03.314.

26. Ojodun, O.E.; Imoisili, P.E.; Jen, T.-C. (2025). Effects of Conductivity Enhancement and Morphological Changes of Nickel Oxide on Supercapacitor Performance: A Review. *Energy Technol.* 13, 2500362. https://doi.org/10.1002/ente.202500362.

27. Panigrahi, K.; Howli, P.; Chattopadhyay, K.K. (2020). 3D network of V2O5 for flexible symmetric supercapacitor. *Electrochimica Acta* 337, 135701. https://doi.org/10.1016/j.electacta.2020.135701.

28. Parvizi, P.; Kazazi, M. (2018). Binder-free copper hexacyanoferrate electrode prepared by pulse galvanostatic electrochemical deposition for aqueous-based Al-ion batteries. *Adv. Ceram. Prog.* 4(2), 27-31. https://doi.org/10.30501/acp.2018.91122.

29. Patil, P.G.; Langade, K.J.; Vyawahare, S.K. (2024). Synthesis and characterisation of PANI and PANI-NiO nanocomposite for promising supercapacitor application. *Ionics* 30, 8369–8378. https://doi.org/10.1007/s11581-024-05827-4.

30. Pawar, P.S.; Salunkhe, A.D.; Pagare, P.K.; Mungase, S.D.; Mujawar, S.H.; Survase, A.A.; Torane, A.P. (2025). Synthesis of homogeneous nickel-cobalt hydroxide nanosheets for supercapacitor application. *Interactions* 246, 89. https://doi.org/10.1007/s10751-025-02315-7.

31. Qazi, U.; Pradeep, H.; Haider, S.; Rosaiah, P.; Ali, R.; Hussain, I.; Shaheen, N.; Akkinepally, B. (2025). Hierarchical Ni(OH)2 Nanoflake-Nanoflower Architectures on 3D Ni Foam for High-Performance Supercapacitors. *Microchem. J.* 219, 116150. https://doi.org/10.1016/j.microc.2025.116150.

32. Shahzad, M.; Ahmad, F.; Ibraheem, M.; Shakoor, A.; Ramay, S.M.; Raza, M.R.; Atiq, S. (2025). Tuning diffusion coefficient, ionic conductivity, and transference number in rGO/BaCoO3 electrode material for optimized supercapacitor energy storage. *RSC Adv.* 15, 6308–6323. https://doi.org/10.1039/d4ra08894h.

33. Shaikh, N.N.; Neamat, R.B.N.; Shaikh, R.H.; Kale, R.B. (2026). Hierarchical 3D nickel oxide microflowers constructed from 2D nanoflakes for supercapacitor applications. *J. Mater. Sci. Mater. Electron.* 37, 1197. https://doi.org/10.1007/s10854-026-17607-z.

34. Torknik, F.S.; Choi, G.M.; Maghsoudipour, A.; Kianpour Rad, M. (2018) Nanostructuring Platinum Nanoparticles on Ni/Ce0.8Gd0.2O2-δ Anode for Low Temperature Solid Oxide Fuel Cell via Single-step Infiltration: A Case Study. *Adv. Ceram. Prog.* 4(1), 45-51. https://doi.org/10.30501/acp.2018.90833.

35. Wang, M.; Zheng, P. (2024). Carbon-Coating Co-Doped α-Ni(OH)2 for High-Performance Supercapacitors. *JOM* 76, 6809–6815. https://doi.org/10.1007/s11837-024-06868-w.

36. Wesley, K.J.S.; Shireesha, K.; Divya, V.; Rakesh, D.; Chakra, C.H.S.; Chandana, K.S.; Reddy, S.S.V.G.; Deepti, K.; Narsaiah, T.B.; Sadhana, K. (2024). Impact of surfactant on specific capacitance of nickel oxide nanoparticles for supercapacitor application. *Bull. Mater. Sci.* 47, 30. https://doi.org/10.1007/s12034-023-03101-3.

37. Wongsaprom, K.; Boonraksa, N.; Pimsawat, A.; Daengsakul, S.; Swatsitang, E. (2025). One-step hydrothermal synthesis of Ni(OH)2/activated rice husk carbon nanocomposites for electrochemical performance enhancement of symmetric supercapacitor. J. *Mater. Sci. Mater. Electron.* 36, 315. https://doi.org/10.1007/s10854-025-14402-0.

38. Wu, M.-S.; Huang, Y.-A.; Yang, C.-H. (2008). Capacitive Behavior of Porous Nickel Oxide/Hydroxide Electrodes with Interconnected Nanoflakes Synthesized by Anodic Electrodeposition. *J. Electrochem. Soc.* 155, A798. https://doi.org/10.1149/1.2969948.

39. Yang, W.-Z.; Liu, Y.-J.; Wang, M.-Y.; Wang, X.; Liu, Q.; Lan, L.; Yin, P.; Zhan, C.-H.; Jiang, Z.-G.; Wang, X. (2025). Giant Five-Shell Polyoxometalate Cages and the Single-Cluster-Based Nanowire Superstructures. *J. Am. Chem. Soc.* 147, 25990–25997. https://doi.org/10.1021/jacs.5c08771.

40. Zhang, Y. (2015). Thermal oxidation fabrication of NiO film for optoelectronic devices. *Appl. Surf. Sci.* 344, 33–37. https://doi.org/10.1016/j.apsusc.2015.03.099.

41. Zhao, J.; Liu, L.; Wang, X.; Gao, W.; Wang, Z.; Zhang, X.; Wang, Y.; Liu, W. (2024). The influence of anionic surfactant (SDS) on the optical, magnetic and capacitive properties of NiO nanocrystals via gas-liquid diffusion synthesis. *Mater. Sci. Eng. B* 299, 116970. https://doi.org/10.1016/j.mseb.2023.116970.

42. Zhou, Q.; Liu, Z.; Qin, X.; Tang, S.; Luo, X. (2025). Atomic Fe–N4/P doped hierarchical porous carbon nanofiber flexible cloth for efficient Zn–air batteries in wide–range temperature. *Carbon* 247, 121034. https://doi.org/10.1016/j.carbon.2025.121034.